Stabilization of External Filter Cake by Colloidal Forces in a "Well–Reservoir" System

A. Kalantariasl and P. Bedrikovetsky*

Australian School of Petroleum, University of Adelaide, Adelaide, South Australia 5005, Australia

ABSTRACT: Growth of an external filter cake with its final stabilization has been widely reported for waterflooding in oilfields, well drilling, fresh water storage, and industrial waste disposal in aquifers. We derive the mechanical equilibrium equation for stabilized cake accounting for electrostatic force and for varying permeate force factor. The main empirical parameter of the model, highly affecting the stabilized cake prediction, is the lever arm ratio for the particle on the cake surface. The lever arm ratio was calculated from laboratory cross-flow filtration experiments and from well injectivity data. It was also determined from Hertz's theory for the elastic particle deformation on the solid cake surface. Good agreement between the results validates the developed mechanical equilibrium model with the lever arm ratio determined from the elastic particle deformation theory.

1. INTRODUCTION

The major fraction of world oil is produced by water flooding, where the injected water displaces oil and maintains the reservoir pressure. Water injection occurs also during the disposal of produced water in aquifers, storage of fresh water in aquifers, disposal of industrial wastes in subterranean formations, etc.[1–3] According to Darcy's law, water flux is proportional to pressure gradient. Therefore, the injected rate is proportional to pressure difference between the well and the reservoir. The proportionality coefficient is called well injectivity index and is the major indicator of well efficiency. Well injectivity decline is described by increasing of the so-called well impedance, which is the normalized inverse to well injectivity index[1]

$$J(t_D) = \frac{q_0}{\Delta p_0} \frac{\Delta p(t)}{q(t)}, \qquad \Delta p = p_w - p_{res} \tag{1}$$

where q is the volumetric well rate, p_w and p_{res} are wellbore and reservoir pressure, respectively, and Δp is the pressure drawdown.

Drastic decline of injectivity index is a widespread phenomenon during the injection of seawater, reinjection of produced water, and injection of any poor quality water. The injected water carries the suspended particles into the reservoir, where they are captured by the rock resulting in permeability decline. When the injected particles plug the inlet reservoir cross section, the formation of low permeable external filter cake occurs (Figure 1a). It yields the decline in well injectivity.

The theory of suspension transport in rocks is a well-developed area of porous media hydrodynamics;[4–7] it provides with the explicit formulas for well injectivity decline.[8–12] Deep bed filtration of aqueous colloids and suspensions is described by the so-called classical filtration theory. Mathematical models have been developed for attachment, straining, and other mechanisms of the particle capture as well as for particle detachment.[1,2,13–15] The system of governing equations for deep bed filtration allows for exact solution in the case of axi symmetric flow of low concentration suspensions. The distinguished feature of the solution is the linear impedance
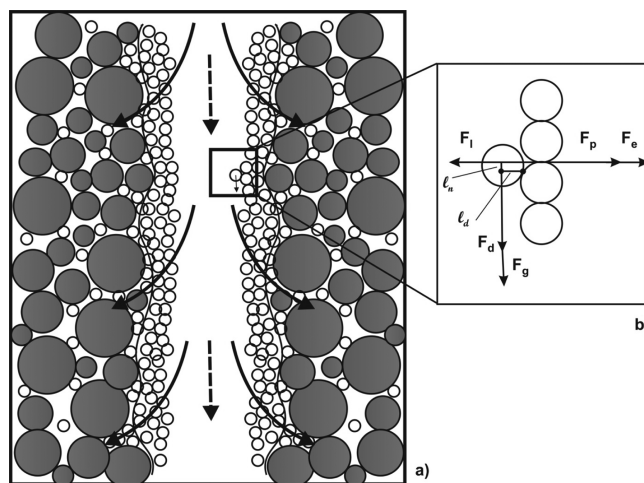

Figure 1. Mechanical equilibrium of particle on the surface of external filter cake on the well wall: (a) deep bed filtration and external filter cake formation during water injection; (b) zoom showing forces exerting the particle.

dependency of the amount of injected particles.[1–3,8,10,12] An analytical model was used for prediction of the injection well behavior and for characterization of the coupled deep bed filtration and cake formation system from well injection history.[8–12,16,17]

Starting from the moment of significant plugging of the sand-face by the captured particles, where the nonplugged pores do not form an infinite cluster anymore, the particles do not penetrate into the formation, and the particles accumulation on the well wall surface in compacted low permeable external filter cake occurs.[1,3,8–12] The assumption of cake incompressibility yields a linear impedance growth versus the amount of injected
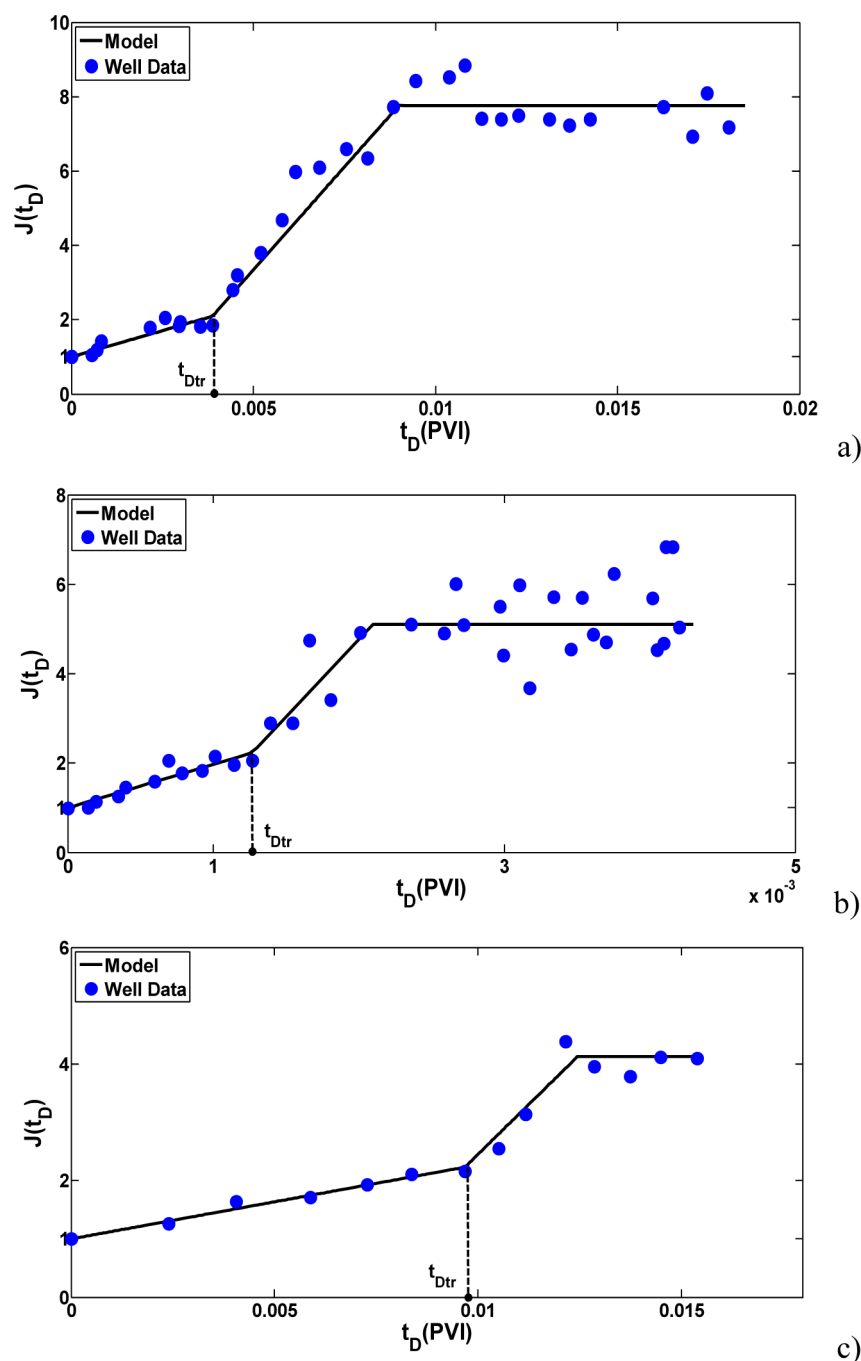
Figure 2. Matching the field data by the analytical model for well injectivity decline: (a) well A (Campos Basin, Brazil); (b) well B (Gulf of Mexico, U.S.A.); (c) well C (LSU, Wyoming, U.S.A.).

particles.[8,10,12,18] The analytical model allows predicting the injection well behavior during the cake formation.

Similar processes occur during drilling of oil, geothermal, and artesian wells: first drilling mud invades the formation, and then the drilling particles form an external filter cake that stabilizes with time due to particle dislodgement.

The external filter cake stabilization after the well injectivity decline has been widely reported in the literature.[10,17,19] The equations for the external filter cake stabilization by different colloidal forces have been presented in refs 18, 20, and 21. Nevertheless, the electrostatic force has been neglected, and the permeate factor variation has been ignored in the model. The above works either do not compare the modeling results with

field and laboratory data or do not interpret the values of the model parameters obtained by the tuning. The stabilized injectivity value and the stabilization time are the most important parameters in the well behavior forecast. However, to the best of our knowledge, the reliable predictive model for stabilized cake is not available in the literature.

In the present work, the mathematical model for stabilization of external cake accounting for electrostatic force and varying permeate factor is developed. The dimensionless analysis of the derived system allows defining the lever arm ratio that is found to be a main parameter determining the stabilized cake. The lever arm ratio was found using the Hertz's theory for the particle deformation on the solid surface. It was also

determined from the laboratory data and well injectivity data. The obtained lever arm ratio values show a good agreement between those predicted theoretically and the laboratory- and field-based values. It validates the model proposed and allows using the model for reliable predictions.

The structure of the paper is as follows. Deep bed filtration and external filter cake formation during water injection are described in Section 2; the main formulas for well impedance are presented in the Appendix. Section 3 presents expressions for all fluid−particle−solid surface forces, which are used in Section 4 in the equation for torque balance equilibrium of the external cake. The lever arm ratio as the main parameter defining the cake stabilization is also introduced in this Section. Section 5 contains determination of the lever arm ratio from well data, from laboratory tests, and from the Hertz particle deformation theory, followed by the comparison of those obtained by the above three methods. Discussion of the model validity and its applications concludes the paper.

2. DEEP BED FILTRATION AND EXTERNAL FILTER CAKE FORMATION

Following papers 4, 8, and 11, in the current Section we briefly describe well injectivity decline due to deep bed filtration of the injected particles and external filter cake formation on the well wall. The increase of injection well impedance is determined by the colloidal phenomena of deep bed filtration in the reservoir following the formation of external filter cake. The typical impedance curve consists of two tilted straight lines and one horizontal line (Figure 2).

Figure 1a shows penetration of the injected particles into porous media with the subsequent capture. The phenomenon is characterized by the filtration coefficient λ, which is the particle capture probability per unit length of its trajectory, and by the formation damage coefficient β that is the increase of reciprocal to permeability per unit concentration of retained particles. The well impedance grows linearly versus time during the particle penetration into the reservoir, see eq A-1 in the Appendix. The slope of the linear dependency $J(t_D)$ is proportional to the formation damage coefficient and to the injected concentration; it also depends on the filtration coefficient. Formulas A-1,2 show that the impedance is proportional to volume of injected particles.

At some moment, the retained concentration reaches the αth fraction of porosity—$\alpha\phi$, which is large enough for the remaining conductive pores not to form an infinite cluster. From this moment on, the injected particles do not penetrate into the rock anymore while the injected carrier water does penetrate. So, the entrance reservoir cross section acts as an ideal filter, allowing water to pass but holding the particles. The value of the corresponding transition time is given by formula A-3 that originates from works 8 and 10. The transition time is determined by the critical porosity ratio α and the filtration coefficient λ.

However, micro-heterogeneity of the rock surface and particle size distribution may cause formation of the cake that does not form a continuous layer.[21] Two simultaneous processes of deep bed filtration and cake formation can occur in this case substituting a simple notion of the transition time.

The particles start forming an external filter cake after the transition time.[8−12] It is assumed that the cake is incompressible. Therefore, volume of the cake is equal to the amount of particles injected since transition time is divided by the volumetric fraction of solid particles in the cake; see eq A-4. It

yields the linear impedance dependency of time, eq A-5. The impedance growth coefficient m_c is proportional to the ratio between the reservoir and cake permeabilities and also to concentration of the injected particles. Since the impedance and cake thickness are linear functions of dimensionless time t_D, the impedance is also a linear function of the cake thickness; see eq A-6. This fact will be used for calculation of the stabilized cake thickness from the stabilized impedance value in Section 5.

Cake compressibility and deep bed filtration of small particles via the large-particle cake yield a nonlinear impedance growth.

Figure 2a,b,c shows raw data of well impedance for three injection wells reported in the papers 10, 17, and 19. The graphs of the increasing impedance curves can be approximated by two piece-wise straight lines with high accuracy; i.e., the well behavior fits well to the mathematical model A-1,5. The impedance stabilizes with time for all three cases shown in Figure 2. The mathematical model for cake stabilization is defined by mechanical equilibrium of a single particle on the cake surface (Figure 1). In the next Section, the forces exerting the particle on the surface of the external filter cake are presented.

3. FORCES EXERTING ON THE PARTICLE AT THE EXTERNAL CAKE SURFACE

Figure 1a shows the stream lines for injected water in the wellbore and in the reservoir. The particles carried by water are deposited at the cake surface after the transition time. A particle on the cake surface is submitted to the drag, permeate, lifting, buoyancy, and electrostatic forces. Figure 1b corresponds to the case of attractive electrostatic force. Electrostatic and permeate forces attach the particles to the surface, while drag, lifting, and gravitational forces detach them.

Drag Force. The expression for drag force exerting the particle on the plane surface is obtained from asymptotic solution of the Navier−Stokes equations by O'Neil[22] and is widely used in modeling of particle attachment and detachment in porous media[1,6,7,13,14,23]

$$F_d = \omega \pi \mu r_s u_t|_{H-r_s} \tag{2}$$

where μ is the viscosity, r_s is the particle radius, H is a half-width of the channel, u_t is the tangential cross-flow velocity of fluid in the center of the particle, and the drag factor ω is equal to 6×1.7. The case of $\omega = 6$ corresponds to the Stokes formula for a particle in the uniform boundary-free flux.[24]

Velocities in the center of the particle situated on the pore wall are

$$u_t|_{H-r_s} = \frac{3r_s\bar{u}}{H}$$
$$u_t|_{r_w-r_s} = \frac{2r_s q}{\pi r_w{}^3} \tag{3}$$

for Hele-Shaw flow in a slot and for Poiseuille flow in tube, respectively.[24] Here $\bar{u}$ is an average velocity through a slot and r_w is well radius. The well rate q is assumed to be a double average cross-flow rate where it linearly decreases from q at the reservoir top to zero at its bottom along the reservoir thickness. Further in the text, formula 3 will be used to interpret the results of laboratory cross-flow filtration tests in the slot and the data of well injectivity decline.

Permeate Force. The expression for a permeate force exerting the particle placed in front of the plane surface of

porous media in the flux perpendicular to the surface is given by the following relationship[23-27]

$$F_p = 6\pi\mu r_s u_p \Phi_H \tag{4}$$

where the permeate factor is given by an empirical formula[25]

$$\Phi_H = 0.36\left(\frac{k_c}{r_s^2}\right)^{-2/5} \tag{5}$$

Here k_c is the cake permeability and $u_p = q/2\pi r_w H_f$ is the permeate velocity on the well wall (at the reservoir entrance). The case $\Phi_H = 1$ corresponds to Stokes formula for the particle in the flux without porous media.

Lifting Force. The lifting force exerting on the spherical particle on the plane surface is[26-33]

$$F_l = \chi(\rho\mu(r_s u_t|_{H-r_s})^3)^{1/2} \tag{6}$$

where different values of the lifting factor are presented for different conditions of the laboratory tests: $\chi = 81.2$ is presented by Bergendahl and Grasso,[27] and Kang et al.;[28] Busnaina et al.,[29] and Burdick et al.[30] give value $\chi = 14$; Altmann and Ripperger[23] gave a value of $\chi = 6.1$; and $\chi = 19.4$ follows from Saffman[31,32] and Akhatov et al.[33]

Buoyancy Force. The net gravitational force exerting the particle in water is

$$F_g = \frac{4}{3}\pi\Delta\rho g r_s^3 \tag{7}$$

Here $\Delta\rho$ is the density difference between the particle matter and carrier water.

Electrostatic Forces. The total electrostatic force is derivative of the overall potential energy

$$F_e = -\frac{\partial V}{\partial h} \tag{8}$$

where the total energy is the sum of the London−van-der-Waals, double electric layer, and Born potentials, given by the so-called DLVO (Derjagin−Landau−Verwey−Overbeek) theory (Derjagin and Landau,[34] Gregory,[35] Elimelech et al.,[36] Khilar and Fogler,[2] and Israelachvili[37])

$$V_{LVA} = -\frac{A_{132}}{6}\left[\frac{2(1+Z)}{Z(2+Z)} + \ln\left(\frac{Z}{2+Z}\right)\right]; \quad Z = \frac{h}{r_s} \tag{9}$$

$$V_{DLR} = \frac{\varepsilon_0 D r_s}{4}\left[2\psi_{01}\psi_{02}\ln\left(\frac{1+\exp(-\kappa h)}{1-\exp(-\kappa h)}\right) - (\psi_{01}^2 + \psi_{02}^2)\right.$$
$$\left.\ln(1-\exp(-2\kappa h))\right] \tag{10}$$

$$V_{BR} = \frac{A_{132}}{7560}\left(\frac{\sigma_{LJ}}{r_s}\right)^6\left[\frac{8+Z}{(2+Z)^7} + \frac{6-Z}{Z^7}\right] \tag{11}$$

$$V = V_{LVA} + V_{DLR} + V_{BR} \tag{12}$$

Here A_{132} is the Hamaker constant, h is the surface-to-surface separation length and Z is its dimensionless value, ε_0 is the electric constant (permittivity of free space), D is the dielectric constant, ψ_{01} and ψ_{02} are the surface potentials of particles and of the cake's matter, respectively, and σ_{LJ} is atomic collision

diameter in Lennard-Jones potential (see Landau and Lifshitz[38]). The inverse Debye length κ is

$$\kappa = \sqrt{\left(\frac{e^2\sum \nu_i z_i^2}{\varepsilon_0 D k_B T}\right)} \tag{13}$$

where k_B is the Boltzman constant, ν_i is a bulk ith ion concentration as defined by the number of ions per unit volume, z_i is a valence of the ith ion, and e is the electron charge $e = 1.6 \times 10^{-19}$ C.

For aqueous solutions under normal temperature, the above formula simplifies as

$$\kappa = 0.73 \times 10^8 \sqrt{\sum C_{mi} z_i^2} \tag{14}$$

where C_{mi} is the molar ith ion concentration in mol/m³ (see Elimelech et al.[36]). The dimension of the constant ahead of the square root in eq 14 is $(m/mol)^{1/2}$.

The particles that are negligibly smaller than the well radius are considered, $r_w \gg r_s$. In this case formula 2 is valid for particles on the cake surface in the plane-parallel flow in the laboratory slot and also in the injection well, although the formulas for calculation of velocity at the particle center $u_t|_{H-r_s}$ via the rate are different for the slot and for well; see eq 3.

Force expressions 2−14 are used in the next Section to determine the conditions of external cake stabilization.

4. MECHANICAL EQUILIBRIUM OF A PARTICLE ON THE CAKE SURFACE

The forces exerting particles on the cake surface are located in the plane crossing the well axes and the particle. The balance for torques of attaching and detaching forces is assumed to be a condition of mechanical equilibrium for a particle on the cake surface in the injected water flux[6,7,13-15,18] (Figure 1b):

$$(F_p + F_e - F_l)l_n = (F_d + F_g)l_d \tag{15}$$

Here l_d and l_n are levers of tangential forces (drag and gravity) and of normal forces (electrostatic, permeate, and lifting).

The criterion 15 defines the critical conditions where the detaching torque exceeds the attaching torque and the fine particle leaves the cake surface. On the contrary, condition 15 states that if the detaching torque does not exceed the attaching torque, the fine particle remains immobile on the cake surface. Since the electrostatic force is a nonmonotonic function of separation distance h, the maximum value of attaching electrostatic force F_e is used in the critical condition 15, i.e., second derivative of the overall potential energy $V = V(h)$ is zero for the separation distance value h in eqs 9−12 that is used for calculation of the electrostatic force in eq 15. See refs 14 and 15 for more detailed discussion.

Permeate, lifting, and drag forces are velocity (well rate) dependent and are independent of water composition, pH, and temperature; see formulas 2−6. On the contrary, the electrostatic force is independent of velocity and strongly depends on the water composition, pH, and temperature; see formulas 8−14. All forces depend on the particle size.

Let us show that lifting force is negligible if compared with permeate force under conditions of injection wells. As it follows from eqs 4−6, the ratio between the lifting and permeate forces depends on Reynolds number
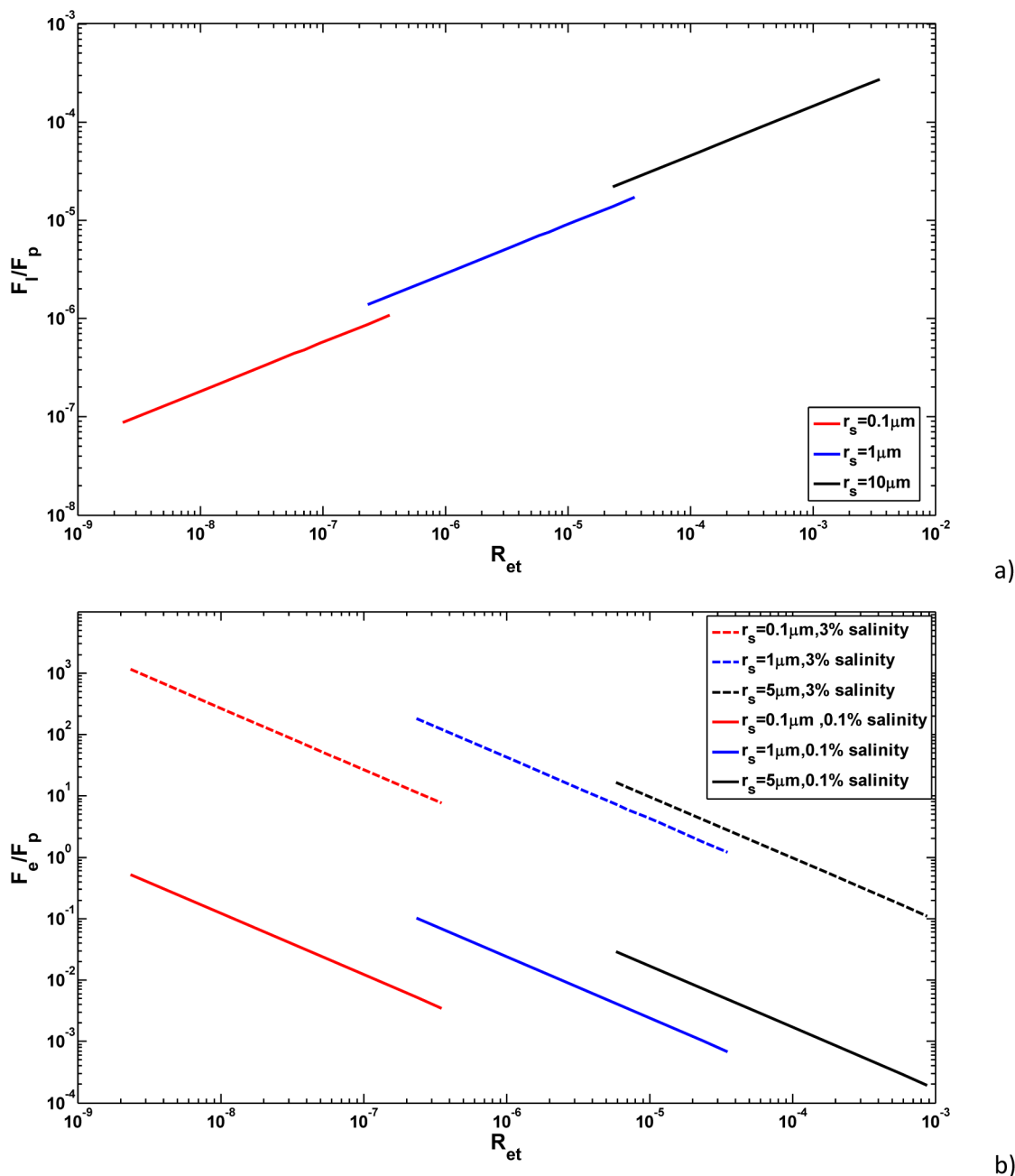
a)

b)

Figure 3. Evaluations of lifting and electrostatic forces if compared with permeate force for water injection conditions: (a) lifting force is negligible if compared with the permeate force; (b) electrostatic force cannot be neglected for high salinity injected water but is negligible for low salinity water.

$$Re_t = \frac{\rho u_t|_{H-r_s} r_s}{\mu} \tag{16}$$

as defined for the particle size r_s.

Figure 3a shows dependency of the lifting-permeate ratio as a function of Reynolds number for different size particles as calculated by eqs 4–6. Since the upper estimate of lifting force must be used to prove that the lifting force is negligible if compared with other forces, the maximum value of lifting factor $\chi = 81.2$ was taken; the permeate factor was calculated by correlation 5. Both forces along with the Reynolds number are monotonically increasing functions of the velocity (rate) and particle size. As it follows from eqs 3, 4, and 6, lifting force is proportional to $q^{3/2}$ while the permeate force is proportional to rate q, so the ratio between lifting and permeate forces is

proportional to $q^{1/2}$. Lifting force is proportional to r_s^3 while the permeate force is proportional to particle size $r_s^{9/5}$, so the ratio between lifting and permeate forces is proportional to $r_s^{6/5}$. As it follows from eqs 3 and 16, Reynolds number is proportional to qr_s^2. Therefore, the lifting-permeate force ratio is proportional to $Re^{1/2}$ at constant particle size. Straight lines in Figure 3a have slope 1/2 in logarithmic coordinates. The larger the particle, the higher the force ratio.

The range of particle sizes as typical for raw and filtered injected waters is 0.1–10 μm. The well rate varies from 0.5 to 80 m^3 per day per meter of the production thickness. The well radius is $r_w = 0.1$ m. The typical value $k_c = 0.1$ md is assumed for cake permeability. It determines the range of Reynolds number variation presented in Figure 3. The ratio F_l/F_p is below 10^{-3} for the overall interval of the Reynolds number
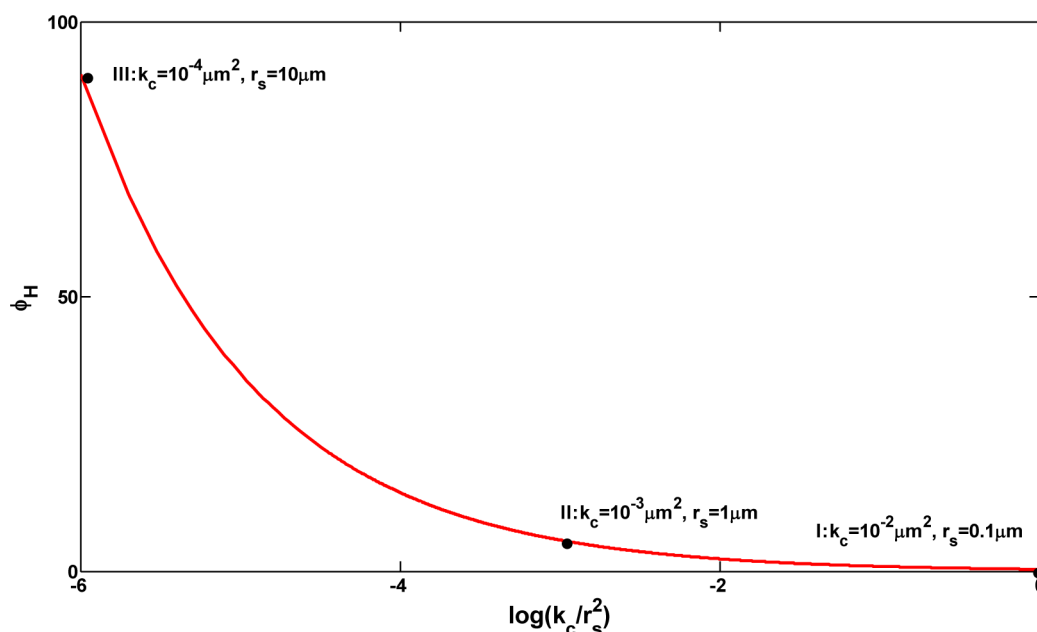
Figure 4. Evaluation of the permeate factor for different cake permeabilities and particle sizes.

variation, so the lifting force can be neglected if compared with the permeate force in formula 15.

Now let us show that electrostatic force can highly exceed the permeate force; i.e., it cannot be neglected in the model of the particle mechanical equilibrium.

The Reynolds number dependency of the ratio between electrostatic and permeate forces is shown in Figure 3b. The electrostatic force is calculated by DLVO formulas 8−14 for the cases of high salinity (3 wt %) and low salinity water (0.1%). The electrostatic force is calculated using three particle radii r_s = 0.1−5 μm that is typical for seawater injection;[10,17,19] the Hamaker constant corresponds to quartz−quartz interaction in aqueous environment A_{132} = 2.0 × 10^{-21} J (see Israelachvili[37]); zeta-potentials for quartz particles and for the cake are $\psi_{01} = \psi_{02}$ = −12 mV correspond to seawater salinity;[39] ε_0 = 8.854 × 10^{-12} C^2 J^{-1} m^{-1} is the permittivity of free space (vacuum); D = 78.0 is the dielectric constant for water (see Khilar and Fogler[2] and Elimelech et al.[36]); atomic collision diameter in Lennard-Jones potential is σ_{LJ} = 0.5 nm (Khilar and Fogler[2]); and the inverse Debye length κ = 2.34 × 10^9 m^{-1} is calculated by eq 14 for seawater with z = 1 for sodium chloride and seawater salinity C_m = 510 mol/m^3. For quartz particles in water with low salinity (0.1 wt %), zeta-potentials for particle and for rock are equal $\psi_{01} = \psi_{02}$ = −50 mV.[40] The inverse Debye length as calculated by eq 14 becomes κ = 1.35 × 10^7 m^{-1} for water with low salinity 0.1 wt %.

Electrostatic force is velocity independent while permeate force is proportional to rate q. Therefore, the electrostatic−permeate force ratio is proportional to Re^{-1} at constant particle size. Straight lines in Figure 3b have slope −1 in logarithmic coordinates. Both electrostatic and lifting forces are monotonically increasing functions of particle size. The calculations show that the larger the particle, the larger the ratio.

Electrostatic force has the same or higher order of magnitude than permeate force for injection of water with 3% salinity (seawater injection), i.e., in the case of strong particle−cake attraction. The electrostatic force can be neglected if compared with permeate forces only for the cases of low salinity water, high injection rates, and large particles.

The above calculations for the permeate force have been performed for the permeate factor as calculated versus the dimensionless cake permeability, see eq 5. The permeate factor value is shown in Figure 4 for different particle sizes and cake permeabilities. The larger the particles and the lower the cake permeability, the higher the permeate factor and permeate force. Three points on the curve correspond to extreme and medium values of particle sizes and cake permeabilities for conditions of the injection wells. The values of the permeate factor highly exceed one. The minimum value is reached for small particles r_s = 0.1 μm and large cake permeability k_c = 10^{-14} m^2 and is equal to 0.36. So, the value of permeate factor can highly exceed unity that yields the significant change in the permeate force. Therefore, the permeate factor variation cannot be neglected.

Substituting the expressions for forces 2, 4, 7, and 8−12 into 15 and neglecting the lifting force yields

$$(6\pi\mu r_s u_p \Phi_H + F_e) = l\left(\omega\pi\mu r_s u_t|_{H-r_s} + \frac{4}{3}\pi\Delta\rho g r_s^3\right),$$

$$l = \frac{l_d}{l_n} \tag{17}$$

The torque balance condition 17 shows that the lever arm ratio l is the only phenomenological parameter in the mechanical equilibrium model provided that the shape factors for drag and lifting forces are known. The next Section is devoted to determination of the lever arm ratio.

5. CALCULATION OF THE LEVER ARM RATIO

In this Section, the methods to obtain the lever arm ratio from the stabilized well impedance and laboratory cross-flow tests and by Hertz theory of particle deformation are developed. Altogether the lever arm ratios are determined from three well histories and from seven laboratory tests. Those ratios as obtained from three different nature tests have the same order of magnitude.

5.1. Determination of the Lever Arm Ratio from Well Data. Let us determine the lever arm ratio from the stabilized

Table 1. Field Data on Well Index Stabilization during Colloidal-Suspension Injection into Oil Reservoirs

well no.	particle radius r_s (μm)	q/H_f (10^{-5} m² s⁻¹)	A_{132} (10^{-21} J)	injection concentration c^0 (ppm)	reservoir permeability k (10^{-15} m²)	formation porosity ϕ	cake porosity ϕ_c	drainage radius r_e (m)
A	3	5.2	2	5	1000	0.28	0.2	500
B	3	4.5	2	3	1036	0.33	0.2	535
C	3	9	2	16	30	0.30	0.2	500

impedance values of injection wells. First, the field data presented in Figure 2 are tuned by the mathematical model of deep bed filtration and external filter cake formation presented in the Appendix. The data from three field cases of well injectivity decline are taken from works by Rickford and Finney,[19] Sharma et al.,[10] and Paiva et al.,[17] where well rates, wellbore, and reservoir pressures are given. The parameters are presented in Table 1. The impedance curves versus dimensionless time are presented in Figure 2. Here the values of relative permeability $k_{rwor} = 0.2$ and water viscosity $\mu = 10^{-3}$ Pa·s are used. The model contains five parameters: filtration λ and formation damage β coefficients, critical porosity fraction α, cake permeability k_c, and the lever ratio l. The average value $\alpha = 0.09$ was taken from works 16 and 17. The filtration coefficient λ was calculated from eq A-3, where the transition time was determined from curves in Figure 2 as a point of cross section of two linear intervals of impedance growth. The formation damage coefficient β was determined from the slope of the impedance straight line during deep bed filtration using eq A-2. Cake permeability k_c was determined from the impedance straight line during cake formation using formula A-5. The results are presented in Table 2. The obtained values of

filtration and formation damage coefficients and cake permeability vary in the common intervals.[1,6−8,16] It allows confirming that the injectivity decline in the three above cases is explained by deep bed filtration of injected solid particles and by formation of the external filter cake.

The stabilized (critical) cake thickness is determined from the stabilized impedance by eqs 17 and A-6.

Substitution of the velocity u_p as calculated from the rate expression and the tangent velocity u_t as obtained from Poiseuille profile into torque balance 17 results in

$$\left(\frac{6\pi\mu r_s \Phi_H}{2\pi H_f (r_w - h_{cr})}q + F_e\right) = l\left(\frac{2\omega\pi\mu r_s^2 q}{\pi(r_w - h_{cr})^3} + \frac{4}{3}\pi\Delta\rho g r_s^3\right) \quad (18)$$

The following data have been collected from the original papers in order to estimate the lever arm ratio from eq 18. Some data are presented in Table 1. The permeate force is calculated using viscosity of low concentration injected suspension that is equal to water viscosity $\mu = 10^{-3}$ Pa·s; well rates per unity of the production thickness q/H_f for three wells have been taken from the original papers and are presented in Table 1; well radii r_w are 0.1, 0.14, and 0.1 m, respectively;[10,17,19] the critical cake thickness h_{cr} is calculated from stabilized impedance value by formula A-6; the permeate factor $\Phi_H = 18.7$, 65.7, and 55.8 is calculated from eq 5 using the cake permeability k_c for three wells A, B, and C as presented in Table 2, respectively. The papers 10, 17, and 19 report seawater injection, so typical 3 wt % of salinity was assumed. The electrostatic force is calculated using particle radius $r_s = 3$ μm that is typical for seawater injection;[10,17,19] Hamaker constant corresponds to quartz−quartz interaction in aqueous

Table 2. Tuning the Analytical Model of Injectivity Impairment from Field Data

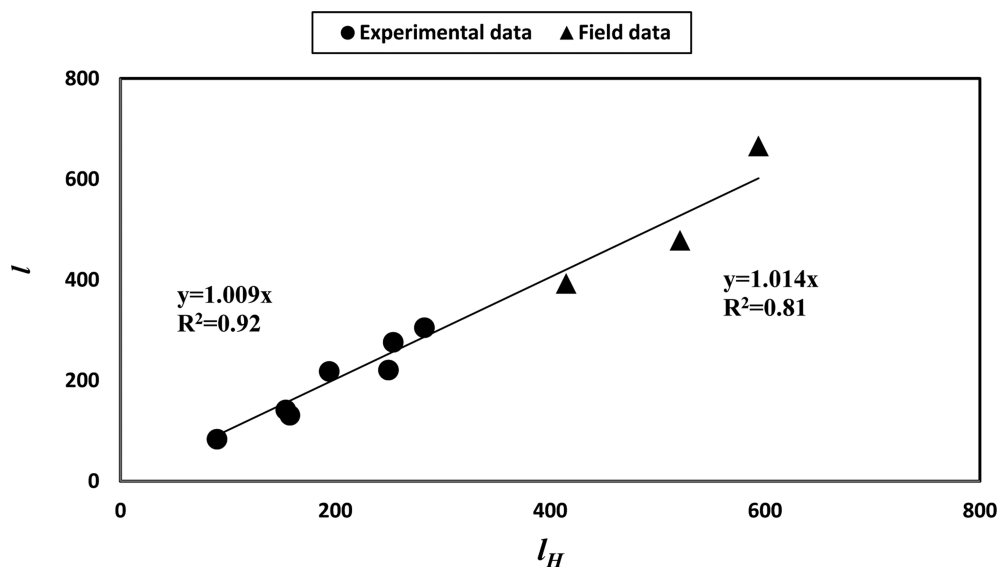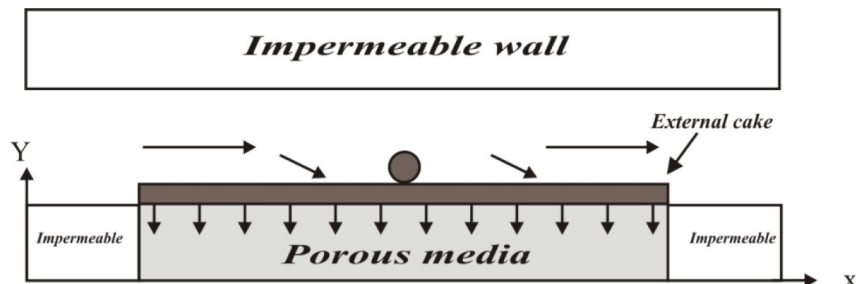| well no.	filtration coefficient λ (m⁻¹)	formation damage coefficient β	cake permeability k_c (10^{-15} m²)	lever arm ratio l
A	4.6	207	0.46	394
B	70	174	0.02	666
C	12.4	20	0.03	478

Figure 5. Interval for lever ratio calculated from lab test and field data: seven ball points correspond to laboratory tests, triangular points l_A, l_B, and l_C are obtained from stabilized well impedance data and points l_{HA}, l_{HB}, and l_{HC} are calculated from Hertz theory.

Table 3. Forces Calculated from Field Data on Well Index Stabilization during Colloidal-Suspension Injection into Oil Reservoirs

well no.	permeate force (F_p, N)	drag force (F_d, N)	lifting force (F_l, N)	electrostatic forces (F_e, N)	gravity force (F_g, N)	normal force (F_n, N)
A	1.11×10^{-10}	1.55×10^{-12}	4.99×10^{-14}	1.20×10^{-9}	1.78×10^{-12}	1.31×10^{-9}
B	2.89×10^{-10}	4.53×10^{-13}	7.90×10^{-15}	1.20×10^{-9}	1.78×10^{-12}	1.49×10^{-9}
C	2.56×10^{-10}	1.26×10^{-12}	3.65×10^{-14}	1.20×10^{-9}	1.78×10^{-12}	1.46×10^{-9}

Figure 6. Schematic of experimental cross-flow filtration.

Table 4. Laboratory Data on Filter Cake Stabilization during Cross-Flow Filtration

experiment no.	particle type	particle diameter (nm)	tangential velocity (m s^{-1})	permeate velocity (10^{-5} m s^{-1})	A_{132} (10^{-21} J)	zeta potential (mV)
1	silica	47	0.246	0.80	2	−31
2	silica	110	0.264	1.08	2	−29
3	silica	80	1.64	1.50	2	−32
4	polystyrene	110	0.116	2.30	3.1	−42
5	polystyrene	760	0.116	2.67	3.4	−42
6	latex	55	0.24	10	4.65	−49
7	silica	480	1	1.25	2	−22

environment (see Israelachvili[37]); $\psi_{01} = -12$ mV and $\psi_{02} = -12$ mV correspond to seawater salinity;[39] $\varepsilon_0 = 8.854 \times 10^{-12}$ C^2 J^{-1} m^{-1} is the permittivity of free space (vacuum); $D = 78.0$ is the dielectric constant for water (see Khilar and Fogler[2] and Elimelech et al.[36]); atomic collision diameter in Lennard-Jones potential is $\sigma_{LJ} = 0.5$ nm (Khilar and Fogler[2]); the inverse Debye length $\kappa = 2.34 \times 10^9$ m^{-1} is calculated by eq 14 for seawater with $z = 1$ for sodium chloride and seawater salinity $C_m = 510$ mol/m^3. The drag factor $\omega = 10.2$ to calculate drag force was taken from ref 22. Since the rate linearly decreases from the well rate at the reservoir top to zero at the reservoir bottom, the average value of $q/2$ is used in formula 3. The particle density used, $\rho = 2600$ kg/m^3, corresponds to quartz particles.

The lever arm ratio results are presented in Figure 5 by triangle points l_A, l_B, and l_C that correspond to wells from Figure 2 a,b,c, respectively. The corresponding lever arm ratios are $l_A = 395$, $l_B = 666$, and $l_C = 478$.

The values of all exerting forces as calculated for the field cases are presented in Table 3. The permeate force highly exceeds the drag force; electrostatic force exceeds them both. Lifting force is negligible. Gravity has the same order of magnitude as drag force for large particles typical for water injection.

5.2. Determination of the Lever Arm Ratio from Laboratory Tests. Let us determine the lever arm ratios from seven experiments presented in works 26 and 40−44. The laboratory cross-flow filtration tests are performed in a rectangular slot with cross-flow into porous sample. The schema of laboratory setup is presented in Figure 6. Water flows via the slot. The inlet and outlet rates have been monitored during tests along the pressure drop across the

porous samples. Assuming incompressibility of the colloidal suspension, the permeate flux was calculated from the difference between the inlet and the outlet fluxes. Tangential velocity was calculated from the inlet rate while the permeate velocity was determined from permeate rate. The above allow calculating the stabilized impedance value. The parameters of the seven investigated tests are presented in Table 4: experiments 1 and 2 correspond to works by Faibish et al.[41] and Hong et al.;[42] experiment 3 was reported by Song and Singh,[43] tests 4 and 5 are presented by Tarabara et al.;[44] test 6 is carried out by Hwang et al.;[26] and experiment 7 was performed by Elzo et al.[40]

Like in the above-mentioned case of three wells, the values of parameters are taken from the original papers; see Table 4. Silica, latex, and polystyrene particles have been used. Hamaker constant values were taken from refs 2, 36, and 37 for given particle and porous media materials.

The flux fraction is directed into the porous medium. The injected particle deposits on the cake surface in the case of attaching torque exceeding the detaching torque. Since the gravity in the vertical slot is vertical and drag force is horizontal, the balance for torques of attaching and detaching forces slightly differs from that given by eq 15:

$$(F_p + F_e - F_l)l_n = \left(\sqrt{F_d^2 + F_g^2}\right)l_d \qquad (19)$$

Substitution of formulas for forces 2, 4, 7, and 8−12 into torque balance 19 results in

$$(6\pi\mu r_s u_p \Phi_H + F_e) = l\left[(\omega\pi\mu r_s u_t|_{H-r_s})^2 + \left(\frac{4}{3}\pi\Delta\rho g r_s^3\right)^2\right]^{1/2} \qquad (20)$$

Table 5. Forces Calculated from Laboratory Data on Filter Cake Stabilization during Cross-Flow Filtration

experiment no.	permeate force (F_p, N)	drag force (F_d, N)	lifting force (F_l, N)	electrostatic forces (F_e, N)	gravity force (F_g, N)	normal force (F_n, N)
1	1.03×10^{-14}	2.97×10^{-14}	7.24×10^{-17}	3.89×10^{-12}	6.86×10^{-19}	3.90×10^{-12}
2	6.40×10^{-14}	1.63×10^{-13}	9.27×10^{-16}	2.17×10^{-11}	8.80×10^{-18}	2.18×10^{-11}
3	7.53×10^{-14}	9.60×10^{-15}	2.44×10^{-17}	2.86×10^{-12}	3.38×10^{-18}	2.94×10^{-12}
4	1.04×10^{-13}	2.65×10^{-15}	3.53×10^{-18}	4.80×10^{-13}	3.43×10^{-19}	5.84×10^{-13}
5	2.94×10^{-12}	1.26×10^{-13}	1.16×10^{-15}	3.20×10^{-11}	1.13×10^{-16}	3.49×10^{-11}
6	6.21×10^{-14}	3.63×10^{-14}	9.76×10^{-17}	2.98×10^{-12}	4.30×10^{-20}	3.04×10^{-12}
7	8.13×10^{-13}	2.15×10^{-12}	8.20×10^{-14}	4.70×10^{-10}	6.85×10^{-16}	4.71×10^{-10}

Here, following O'Neill,[22] $\omega = 6 \times 1.7$.

Calculation of tangential velocity in the center of the particle from Couette velocity profile yields the transcendental equation for the stabilized cake thickness

$$(6\pi\mu r_s u_p \Phi_H + F_e) = l\left(\left(\frac{3\omega\pi\mu r_s^2 \overline{u}_t}{H - h_{cr}}\right)^2 + \left(\frac{4}{3}\pi\Delta\rho g r_s^3\right)^2\right)^{1/2} \tag{21}$$

This thickness is measured during the laboratory tests. Like in the discussed above case of flow in the vertical tube, in the case of plane-parallel flow in laboratory slot, eq 21 determines the empirical parameter l.

Figure 5 shows the lever arm ratios as obtained from seven laboratory studies. The tests followed the schematic in Figure 6.

The laboratory-based values of the lever arm ratio vary in the interval 84−305.

Table 5 shows the values for all forces as calculated for seven laboratory tests. Drag and permeate forces have the same order of magnitude. Lifting and gravitational forces are negligible. The electrostatic forces are 2 orders of magnitude higher than both drag and permeate forces; it explains high obtained values of the lever arm ratio.

5.3. Determination of the Lever Arm Ratio from the Contact Particle Deformation. Following works 1, 6, 7, and 14, let us determine the lever arm ratio from the deformation of the elastic particle on the cake surface by the total normal force. The total of permeate, electrostatic, and lifting forces deforms a particle and creates a tangent area on the particle−cake contact. Since cake permeabilities are extremely low (see the interval 0.02−0.5 md for cake permeability in Table 2), it is possible to assume that the cake is highly consolidated and its surface is a flat solid surface where the particle deformation schematic applies. It is assumed that the particle rotates around the boundary of the deformed area at the moment of the particle lifting, so the lever arm for normal force is equal to radius of the contact area. Figure 7a presents the compressible particle deformed by the attaching normal force and shows how the infinitesimal particle rotates at the moment of its mobilization. The Hertz's theory presents with the explicit formula for radius of the contact area which is equal to the normal lever l_n. It was originally derived by Derjagin et al.[45] for the case of particle deformed by electrostatic force and was used for the colloidal particles attached to solid surface:[1,6,7,13,27]

$$l_n = \left(\frac{(F_e + F_p - F_l)r_s}{K}\right)^{1/3} \tag{22}$$

Here, K is the composite Young modulus that depends on the Poisson's ratio σ and Young's elasticity modulus E of the particle and of the cake
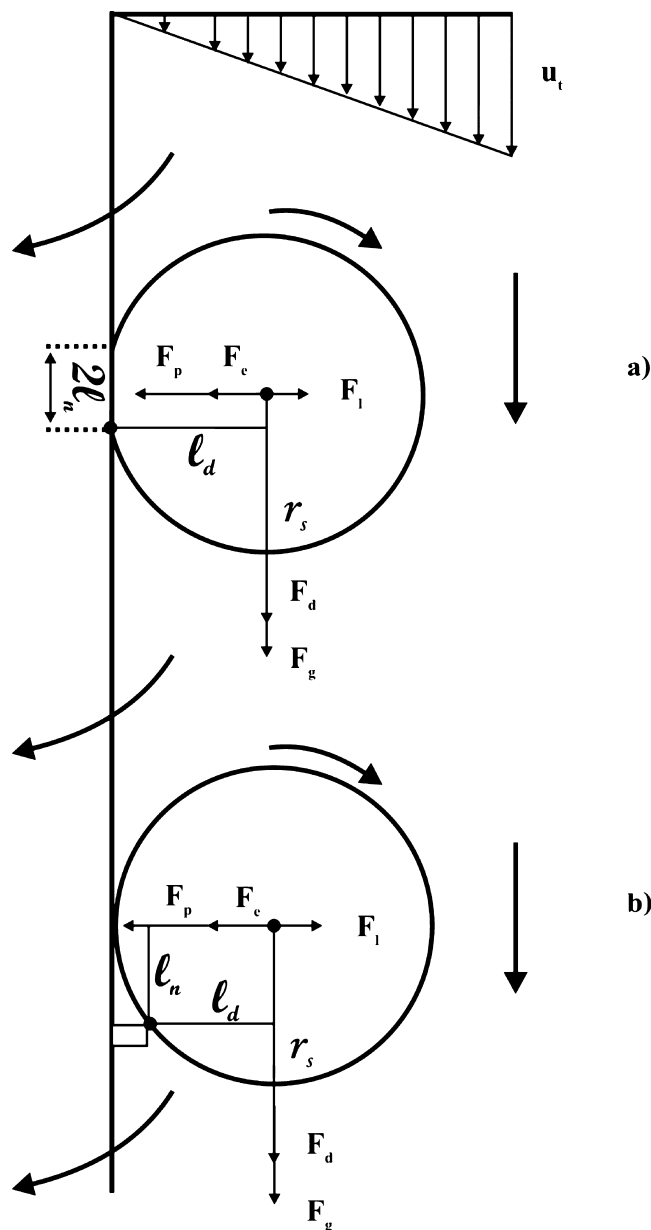

Figure 7. Schematic for torque balance exerting the particle at the moment before mobilization: (a) lever arm is equal to the size of deformed particle−cake contact area; (b) lever arm is equal to the distance to the supporting asperity.

$$K = \frac{4}{3}\left(\frac{(1 - \sigma_s^2)}{E_s} + \frac{(1 - \sigma_c^2)}{E_c}\right)^{-1} \tag{23}$$

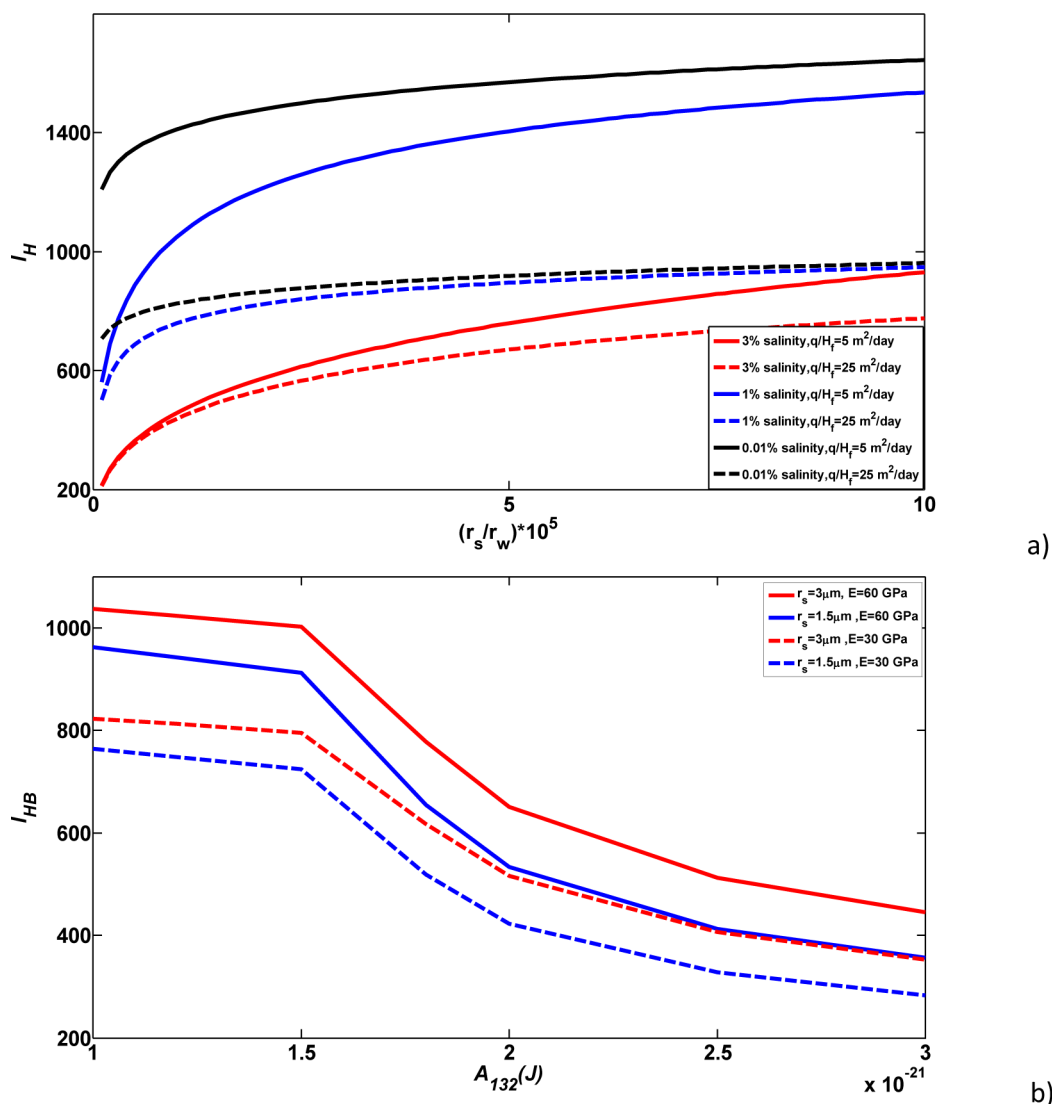where subscripts s and c refer to particle and cake, respectively.

a)

b)

Figure 8. Sensitivity study and the typical variation interval for the lever arm ratio under the injection well conditions.

For rigid sandstone particles like quartz or silica, the contact area size is significantly smaller than the particle radius, $l_n \ll r_s$ (see Schechter[1]). Consider the right-angled triangle formed by two levers and the radius of the upper particle in Figure 7. Since one leg highly exceeds another leg, the large leg is almost equal to the hypotenuse. Therefore, the drag force lever arm can be assumed to be equal to the particle radius. It allows calculating the lever arm ratio using eqs 22 and 23:

$$l_H = \left(\frac{4r_s^2}{3(F_e + F_p - F_l)\left(\frac{(1-\sigma_s^2)}{E_s} + \frac{(1-\sigma_c^2)}{E_c} \right)} \right)^{1/3} \quad (24)$$

The dimensionless lever arm ratios have been calculated for the above-described three field cases. We assume that Young's modulus and Poisson's ratio are equal for particle and cake. Formula 24 becomes simplified for the case where the cake and particle have the same properties

$$l_H = \left(\frac{2Er_s^2}{3(F_e + F_p - F_l)(1 - \sigma^2)} \right)^{1/3} \quad (25)$$

The typical values of Young's modulus and Poisson's ratio for silica particles used in the calculations are $E = 40$ GPa, $\sigma = 0.15$.[1]

The results of calculations of lever arm ratio l_H for three wells are $l_{AH} = 415$, $l_{BH} = 594$, and $l_{CH} = 521$ for wells A, B, and C, respectively.

The obtained values for lever arm ratio are shown by three points in Figure 5. Here the abscissa of each point corresponds to the lever arm ratio obtained from Hertz theory and the ordinates are equal to l-values calculated from well data using eq 18. The points are located close to the bisectrix of the first coordinate angle, which shows good agreement between the well-data-based values of the lever arm ratio and that obtained from Hertz theory.

The lever arm ratios have been also obtained for the conditions of the seven above laboratory tests from Hertz theory 24 and put in a plane in Figure 5 along with the lever arm ratios obtained from the torque balance condition 21. The seven points are also located close to the bisectrix, suggesting good agreement between the laboratory-data-based values of the lever arm ratio and that obtained from Hertz theory.

The lever arm ratios calculated from well data have the same order of magnitude as those obtained from the laboratory tests.

Finally, the elastic particle deformation on the solid plane surface of the cake explains high values of lever ratios as obtained from both injection well and laboratory tests data.

Now let us discuss the variation range for the lever arm ratio. The ratio values l_H have been calculated using the model 25 for parameters typical for injection wells in sandstone offshore and onshore oilfields, like discussed in the above field cases A, B, and C (see Table 1 for the constants used). Figure 8a shows the ratio dependency of the dimensionless particle size, where r_s varies from 0.1 to 10 μm. High, moderate, and low salinity cases are discussed (3.0, 1.0, and 0.01 wt %) for injection rate varying from 5 to 25 m^3 per day per meter of the production thickness. The main affecting parameter is salinity. The electrostatic force is 20 times stronger for high salinity water than in the case of moderate salinity. The higher the salinity, the higher the attracting electrostatic force and the larger the lever for the normal force; i.e., the lever arm ratio is lower. The lever arm ratio as obtained for 3% water is twice lower than for moderate salinity water. The lever arm ratio sensitivity to rate variation is low—fivefold rate variation yields relative lever arm variation 0.15−0.5.

Figure 8b shows the dependency of the lever arm ratio of the Hamaker constant for different particle radii and Young's modulus. The constants in eq 25 correspond to well B. Hamaker constant is the most influential parameter: in the typical range of its variation for silica and quartz $1-3 \times 10^{-21}$ J, the lever arm ratio changes 2−3 times. Variation of l_H for typical variation intervals of particle radius and Young's modulus is significantly lower—the ratio between the l_H variation and its mean value has order of magnitude 0.1. The same order of magnitude for the ratio between the l_H variation and its mean value is obtained from Figure 8a too.

5.4. Role of Roughness and of the Granular Cake Structure.
Figure 7a,b shows the particle compressed by normal force (upper particle) and that rotating around the rock surface asperity during its lifting (lower particle). It is assumed that the particle rotates around the touching point with the surface at the last moment before its mobilization. The lever for the normal force in the upper case is determined from elastic deformation of the particle and surface.

The lever for the normal force in the lower case in Figue 7b is determined by the asperity height. The horizontal distance between the tangent point and the asperity l_n is random and can vary from zero to the particle radius, so the lever arm ratio can randomly vary from infinity to one. The typical asperity size can have the order of magnitude of the particle size. In this case, the lever arm ratio would have order of magnitude of unity. The laboratory- and field-data-based values of the lever arm ratio vary in a relatively narrow interval, i.e., between 84 and 666 (Figure 5); i.e., the lever as obtained by Hetrz theory calculations is significantly smaller than the particle size. Therefore, the asperity of the rough cake surface cannot explain systematically high values of the lever arm ratios.

6. DISCUSSION
Decline of the injection well index in aquifers and oilfields is determined by colloidal-suspension effects of deep bed filtration in porous media, formation of the external filter cake on the well wall, and cake stabilization upon reaching the mechanical equilibrium of a particle on the external cake surface. Field data exhibit a typical form of the well impedance curve consisting of the linear growth from unity during deep bed filtration and linear growth during formation of the external filter cake

followed by a constant value for the stabilized impedance. The first two dynamic stages of well impairment are described by the mathematical models that exhibit a good fit to the presented field cases for the typical values for the matched parameters.

The mechanical equilibrium of a particle on the external cake surface in an injection well is described by the equality of torque balance for attaching and detaching forces. Permeate and electrostatic forces attach particles to the cake while lifting and drag and gravitational forces detach them. The torque balance condition contains an empirical constant—lever arm ratio l, which is a phenomenological parameter of the mechanical equilibrium model. Treatment of seven laboratory tests on cross-flow filtration provides the lever ratios varying from 84 to 305, while three well treatments exhibit the interval 394−666. So, the intervals of the lever ratio variation from the well data and laboratory tests have the same order of magnitude (Figure 5). The difference between the intervals can be explained by different materials and shapes of the particles that have not been reported in the corresponding papers and may affect the values of the obtained l-values. Nevertheless, close values for two intervals validate the torque balance model for the cake stabilization phenomenon.

Several other works presented the lever ratio of the order of magnitude that significantly deviates from the above-mentioned intervals: Paiva et al.[17] calculated $l = 0.05$ by comparison with experimental data;[18,23,42] the parameters used by Al-Abduwani et al.,[21] Zinati et al.,[20] and Yuan et al.[49] correspond to $l = 5.0$, $l = 5.0$, and 2.0, respectively. The reason for this deviation is ignoring the electrostatic force and assuming the unit value for the permeate force correction factor Φ_H. The data treatment of the laboratory tests and the field data accounting for electrostatic force and for jamming ratio dependency of the permeate force correction factor Φ_H yields the lever ratio variation interval 84−666.

Jiao and Sharma[18] assumed that the mono-sized particles form packed hexagonal structure in the cake (Figure 1b). So the lever arm ratio is calculated from equilateral triangle and equals $3^{1/2}$; this value highly differs from the values obtained from the laboratory and well data. This significant difference is explained by the fact that the lever arm ratio is determined by particle and cake deformation rather than by the packed-sphere structure of the cake.

The lever arm ratios for conditions of seven laboratory cross-flow filtration experiments and three well injections have been calculated from the Hertz's theory of elastic sphere deformation on the solid surface by the normal attaching force exerting the sphere (eq 25). The lever arm ratios obtained from the elastic deformation model coincide with those obtained from the mechanical equilibrium conditions with reasonable accuracy (see values of R^2 in Figure 5). The agreement validates the hypothesis that the lever arm ratio is determined by the elastic particle deformation on the solid cake surface. The lever arm ratio depends on the particle size and on Young's moduli and Poisson's ratios for particle and cake.

The asperities of the cake surface are random while the agreement between Hertz-based calculations and lab and well data is regular. It allows concluding that the lever arm ratio is determined by elastic deformation of particles rather than by the rock surface asperities.

Finally, the above allows concluding the validity of the torque balance model for description of the external filter cake stabilization, where the lever arm ratio is determined by the

940

dx.doi.org/10.1021/ie402812y | *Ind. Eng. Chem. Res.* 2014, 53, 930−944

elastic particle deformation. This conclusion supports the prediction of the stabilized injectivity value using the model 24. The validity of this conclusion can be increased by the laboratory tests that repeat the well conditions, i.e., using the same particles as during the water injection cases. The complexity of collecting the borehole samples of the injecting water makes performing the tests very difficult.

Uncertainty in determining the physics constants in the model 24 decreases the accuracy of the stabilized injectivity prediction. It also introduces the uncertainty of interpretation of laboratory and field data (Figure 5). The Hamaker constant, zeta-potential, and particle size are often unavailable not only for injection wells but also for laboratory conditions.[10,17,19,26,40−44] The detailed sensitivity analysis of the lever arm ratio with respect to the constants would increase the validity of the contact deformation model 24 and increase the accuracy of the predictive model. It would also define the measurements that are necessary to perform during the laboratory and field studies.

Some sensitivity results are presented in Figure 8. The Hamaker constant is the most influential parameter in predicting the lever arm ratio. The sensitivities of particle size and Young's modulus are significantly lower.

The proposed lever arm model 17 uses Hertz's formulas 22 and 23 which were derived for a flat cake surface. Low values for obtained cake permeabilities, presented in Table 2, suggest a highly compacted arrangement of deformable particles in the cake. Yet, the schematic of the particle placement on the rock surface (Figure 1b) contradicts the flat surface assumption. Introduction of a shape factor into the contact deformation eqs 22 and 23 may improve the quality of matching between the stabilized impedance values and the mechanical equilibrium model 17 (Figure 5). It may also decrease the interval for possible values of the phenomenological lever arm ratio *l*.

The proposed model assumes the injection of mono-size suspension, resulting in the same stabilization velocity for all particles. However, the injected particles are size-distributed. Therefore, some small particles keep attaching to the cake surface while some large particles are already in equilibrium and do not contribute to cake formation anymore. Selective particle attachment with time should be described by a more complex mathematical model.

The dynamic detachment of large particles during increasing of the injection rate also cannot be described by the proposed model.

The proposed formulas for lever arm ratio along with formulas for deep bed filtration and external cake formation form an analytical predictive model for well index during water injection or well drilling. The mechanical equilibrium model 17 would contain a geometric factor for the cases of fractured, horizontal, slant, or combined horizontal injection wells with fractures. With application of the model 17 to stabilization of the mud cake during drilling, non-Newtonian properties of drilling fluid must be accounted for in expressions 2, 4, and 6 for drag, permeate, and lifting forces, respectively.

However, some important generalizations of the model should be mentioned. During the drilling or water injection in fractured-porous reservoirs, the injected flux enters both fractures and matrix, so the deep bed filtration model in fractured-porous media should be used for well performance prediction.[50,51] High rate water injection could cause the appearance of oil−water emulsion near the wellbore, causing additional injectivity damage; the corresponding mathematical

model for deep bed filtration must include three-phase equations of mass transfer (see refs 3, 52, and 53). More detailed modeling of deep bed filtration accounting for DLVO forces on the microscale can be performed by direct numerical simulation.[54] More complex mass transfer processes rather than a simple particle accumulation occur on the cake surface: cross-flow filtration through the cake, shear-induced diffusion, selective particle deposition according to particle size, charge, etc.[47,48,55]

7. CONCLUSIONS

Derivation of the cake mechanical equilibrium equation accounting for electrostatic force and for varying permeate force correction factor and comparing the modeling results with experimental and field data allow drawing the following conclusions:

Electrostatic force attaching the particle to the external cake surface can highly exceed other forces and significantly change the value of the stabilized cake thickness.

The permeate force correction factor varies up to 3 orders of magnitude under well conditions and highly affects the predicted value of the stabilized cake.

The lifting force is negligible if compared with permeate and drag forces for the well injectivity conditions.

The main empirical parameter affecting the stabilized cake prediction is the lever arm ratio.

Close variation intervals for the lever arm ratio, as obtained from the stabilized well impedance and from the laboratory cross-flow experiments, validate the torque balance equilibrium model.

Good agreement between the predicted values of the lever arm ratio by the Hertz theory and from laboratory and field data suggests that the cake mechanical equilibrium is determined by particle deformation rather than by the well surface asperity.

■ APPENDIX A. IMPEDANCE GROWTH DURING DEEP BED FILTRATION AND EXTERNAL FILTER CAKE FORMATION

Following papers by Pang and Sharma,[8] Barkman and Davidson,[9] Bedrikovetsky et al.,[11] and Ochi et al.,[12] let us present the analytical model for injectivity impairment. The above modeling works assume low retained particle concentration leading to constant filtration and formation damage coefficients. Under these assumptions, well impedance grows linearly during deep bed filtration of the injected particles in the reservoir:

$$J(t_D) = 1 + m t_D, \qquad t_D = \frac{\int_0^t q(t)\, dt}{\pi r_e^2 \phi H_f} \tag{A-1}$$

where t_D is dimensionless time, r_e is a typical distance between wells (drainage radius), ϕ is formation porosity, and H_f is a reservoir thickness.

The slope m in linear dependency of the impedance versus dimensionless time is determined by the values of filtration coefficient λ and formation damage coefficient β

$$m = \frac{\beta\phi c^0(\lambda r_e)^2}{2\ln\frac{r_e}{r_w}}\left(\frac{1}{\lambda r_w} + e^{\lambda r_w}ei(\lambda r_w)\right),$$

$$ei(x) = \int_x^\infty \frac{e^{-y}}{y}\,dy \tag{A-2}$$

Here r_w is well radius and c^0 is the concentration of particles in the injected water.

The empirical filtration and formation damage coefficients λ and β can be estimated from either corefloods or microscale empirical filtration theory.[6,7,46]

By definition of the transition time t_{Dtr}, the deposited concentration at the transition time is equal to the αth fraction of porosity, resulting in the following expression for transition time:

$$t_{Dtr} = \frac{2\alpha X_w}{\lambda r_w c^0}, \quad X_w = \left(\frac{r_w}{r_e}\right)^2 \tag{A-3}$$

The value $\alpha = 0.5$ was used in work 8; laboratory tests suggest $\alpha = 0.09$.[11,16]

The thickness of the incompressible cake is proportional to the amount of injected particles after the transition time[8–12,47,48]

$$h_c(t_D) = \frac{\phi r_e^2 c^0(t_D - t_{Dtr})}{2r_w(1-\phi_c)} \tag{A-4}$$

which also corresponds to the linear impedance growth

$$J(t_D) = 1 + mt_{Dtr} + m_c(t_D - t_{Dtr}),$$
$$m_c = \frac{kk_{rwor}c^0\phi}{2X_w k_c(1-\phi_c)(-\ln X_w)} \tag{A-5}$$

where k is the reservoir permeability, k_{rwor} is relative permeability for water at the presence of residual oil, k_c is the permeability of external filter cake, and ϕ_c is the cake porosity.

The impedance during the cake growth can be expressed via the cake thickness by substitution of eq A-4 into A-5:

$$J(t_D) = 1 + mt_{Dtr} + m_c\frac{2r_w(1-\phi_c)}{\phi r_e^2 c^0}h_c(t_D) \tag{A-6}$$

Typical type curves for impedance/skin growth during injection of water with solid and liquid particles into oilfields are shown in Figure 2.

■ **AUTHOR INFORMATION**

Corresponding Author
*E-mail: pavel@asp.adelaide.edu.au.

Notes
The authors declare no competing financial interest.

■ **NOMENCLATURE**

A_{132} = Hamaker constant, ML^{2}T^{-2}, J
C_m = Molar concentration of ith ion, mol m^{-3}
c^0 = Injected suspended particle concentration
D = Dielectric constant
E = Young's modulus, ML^{-1}T^{-2}, N m^{-2}
F_d = Drag force, MLT^{-2}, N
F_e = Electrostatic force, MLT^{-2}, N
F_g = Gravitational force, MLT^{-2}, N
F_l = Lifting force, MLT^{-2}, N

F_p = Permeate force, MLT^{-2}, N
H = Half-width of the channel, L, m
H_f = Reservoir thickness, L, m
h = Separation distance, L, m
h_c = External cake thickness, L, m
h_{cr} = Stabilized external cake thickness, L, m
II = Injectivity index, L^{4}T^{2}M^{-1}, m^4 s^2 kg^{-1}
J = Impedance
K = Composite Young modulus, ML^{-1}T^{-2}, N m^{-2}
k = Absolute permeability, L^2, m^2
k_B = Boltzmann constant, M L^2 T^{-2} K^{-1}
k_c = External cake permeability, L^2, m^2
k_{rwor} = Water relative permeability at residual oil saturation
l = Lever arm ratio
l_d = Lever arm for tangential forces, L, m
l_H = Lever arm ratio form Hertz deformation theory
l_n = Lever arm for normal forces, L, m
m = Slope of impedance growth during deep bed filtration
m_c = Slope of impedance growth during cake formation
p = Pressure, ML^{-1}T^{-2}, N m^{-2}
q = Total injection rate, L^{3}T^{-1}, m^3 s^{-1}
r_e = Reservoir radius, L, m
R_{et} = Reynolds number
r_s = Particle radius, L, m
r_w = Well radius, L, m
T = Absolute temperature, K
t = Time, T, s
t_D = Dimensionless time (PVI)
t_{Dtr} = Dimensionless transition time (PVI)
u_p = Permeate velocity, LT^{-1}, m s^{-1}
u_t = Tangential velocity, LT^{-1}, m s^{-1}
$\bar{u}$ = Average tangential velocity, LT^{-1}, m s^{-1}
V = Energy of interaction, ML^{2}T^{-2}
X_w = Dimensionless radius
z = Valence of the ith ion
Z = Ratio between the cake surface−particle separation distance and particle radius

Greek letters

α = Critical porosity fraction
β = Formation damage coefficient
ε_0 = Free space permittivity, C^{2}J^{-1}L^{-1}
κ = Inverse Debye length, L^{-1}, m^{-1}
λ = Filtration coefficient, L^{-1}, m^{-1}
μ = Dynamic viscosity, ML^{-1}T^{-1}, kg m^{-1} s^{-1}
ν = Number concentration of the ith ion far away from the surface, L^{-3}
σ = Poisson's ratio
ρ = Density of carrier fluid, ML^{-3}, kg m^{-3}
Δp = Pressure drawdown, ML^{-1}T^{-2}, N m^{-2}
$\Delta\rho$ = Density difference between particle and carrier fluid, ML^{-3}, kg m^{-3}
σ_{LJ} = Atomic collision diameter, L, m
ϕ = Formation porosity
ϕ_c = Cake porosity
Φ_H = Permeate force factor
χ = Lifting force coefficient
ψ = Surface potential, ML^{2}T^{-2}, mV
ω = Drag force coefficient

Abbreviations
PVI = Pore volume injected

Subscripts
BR = Born repulsion (for energy potential)

c = Cake
d = Drag
DLR = Double layer repulsion (for energy potential)
e = Electric
g = Gravity
l = Lifting
i = Index for ion
LVA = London−van der Waals (for energy potential)
n = Normal
p = Permeate
res = Reservoir
s = Solid particle
w = Well
0 = Initial condition or initial value (for flow rate and pressure drop)

■ REFERENCES

(1) Schechter, R. S. *Oil Well Stimulation*; Prentice Hall: New Jersey, 1992.

(2) Khilar, K. C.; Fogler, S. *Migration of Fines in Porous Media*; Kluwer Academic Publishers: Dordrecht, 1998.

(3) Bedrikovetsky, P. *Mathematical theory of oil and gas recovery: with applications to ex-USSR oil and gas fields*; Kluwer Academic Publishers: Dordrecht,1990.

(4) Herzig, J. P.; Leclerc, D. M.; Le Goff, P. Flow of suspensions through porous media—application to deep Filtration. *Ind. Eng. Chem.* 1970, 65, 8−35.

(5) Freitas, A. M.; Sharma, M. M. Detachment of particles from surfaces: an AFM study. *J. Colloid Interface Sci.* 2001, 233, 73−82.

(6) Bradford, S. A.; Torkzaban, S. Colloid transport and retention in unsaturated porous media: A review of interface-, collector-, and pore-scale processes and models. *Vadose Zone J.* 2008, 7, 667−681.

(7) Torkzaban, S.; Bradford, S. A.; Walker, S. L. Resolving the coupled effects of hydrodynamics and DLVO forces on colloid attachment in porous media. *Langmuir* 2007, 23, 9652−9660.

(8) Pang, S.; Sharma, M. M. A model for predicting injectivity decline in water injection wells. *SPE Form. Eval.* 1997, 12, 194−201.

(9) Barkman, J. H.; Davidson, D. H. Measuring water quality and predicting well impairment. *J. Pet. Technol.* 1972, 24, 865−873.

(10) Sharma, M.; Shutong, P.; Wennberg, K. E.; Morgenthaler, L. N. Injectivity Decline in Water-Injection Wells: An Offshore Gulf of Mexico Case Study. *SPE Prod. Facil.* 2000, 15, 6−13.

(11) Bedrikovtsky, P.; da Silva, M. J.; Fonseca, D. R.; da Silva, M. F.; Siqueira, A. G.; Souza, A.; Furtado, C. Well-History-Based Prediction of Injectivity Decline During Seawater Flooding. SPE 93886, Presented at SPE European Formation Damage Conference, Scheveningen, The Netherlands, May 25−27, 2005.

(12) Ochi, J.; Rivet, P.; Lacourie,Y. External filter cake properties during injection of produced waters. SPE 54773, Presented at European Formation Damage Conference, The Hague, Netherlands, May 31−June 1, 1999.

(13) Bergendahl, J. A.; Grasso, D. Mechanistic basis for particle detachment from granular media. *Environ. Sci. Technol.* 2003, 37, 2317−2322.

(14) Bedrikovetsky, P.; Siqueira, F. D.; Furtado, C. A.; Souza, A. L. S. Modified particle detachment model for colloidal transport in porous media. *Transp. Porous Media* 2011, 86, 353−383.

(15) Bedrikovetsky, P.; Zeinijahromi, A.; Siqueira, F. D.; Furtado, C. A.; Souza, A. L. S. Particle detachment under velocity alternation during suspension transport in porous media. *Transp. Porous Media* 2012, 91, 173−197.

(16) da Silva, M.; Bedrikovetsky, P.; Van den Broek, W. M. G. T.; Siqueira, A.; de Souza, A. L. A New Method for Injectivity Impairment Characterization From Well and Coreflood Data. SPE 89885, Presented at SPE Annual Technical Conference and Exhibition, Houston, TX, September 26−29, 2004.

(17) Paiva, R.; Bedrikovetsky, P.; Siqueira, A. G.; Souza, A. L. S. ; Shecaira, F. S. A Comprehensive Model for Injectivity Decline Prediction during PWRI. SPE 100334, Presented at SPE/EAGE Annual Conference and Exhibition, Vienna, Austria, June 12−15, 2006.

(18) Jiao, D.; Sharma, M. M. Mechanism of cake buildup in crossflow filtration of colloidal suspensions. *J. Colloid Interface Sci.* 1994, 162, 454−462.

(19) Rickford, R. L.; Finney, T. P. Formation Damage From Fine Particulate Invasion: An Example From the Lost Soldier Tensleep Formation. *SPE Prod. Eng.* 1991, 6, 247−251.

(20) Zinati, F. F.; Farajzadeh, R.; Currie, P. K.; Zitha, P. L. J. Modeling of external filter cake build-up in radial geometry. *Pet. Sci. Technol.* 2009, 27, 746−763.

(21) Al-Abduwani, F.; Bedrikovetsky, P.; Farajzadeh, R.; van den Broek, W. M. G. T.; Currie, P. K. External filter cake erosion: mathematical model and experimental study. SPE 94635, Presented at SPE European Formation Damage Conference, Scheveningen, The Netherlands, May 25−27, 2005.

(22) O'Neill, M. E. A sphere in contact with a plane wall in a slow linear shear flow. *Chem. Eng. Sci.* 1968, 23, 1293−1298.

(23) Altmann, J.; Ripperger, S. Particle deposition and layer formation at the crossflow microfiltration. *J. Membr. Sci.* 1997, 124, 119−128.

(24) Landau, L. D.; Lifshitz, E. M. *Fluid Mechanics*, 2nd ed.; Pergamon Press: Oxford, 1987; Course in Theoretical Physics, Vol. 6.

(25) Sherwood, J. D. The force on a sphere pulled away from a permeable half-space. *Physicochem. Hydrodyn.* 1988, 10, 3−12.

(26) Hwang, S. J.; Chang, D. J.; Chen, C. H. Steady State permeate flux for particle cross-flow filtration. *Chem. Eng. J.* 1996, 61, 171−178.

(27) Bergendahl, J.; Grasso, D. Prediction of colloid detachment in a model porous media: hydrodynamics. *Chem. Eng. Sci.* 2000, 55, 1523−1532.

(28) Kang, S. T.; Subramani, A.; Hoek, E.; Deshusses, M. A.; Matsumoto, M. R. Direct observation of biofouling in cross-flow microfiltration: mechanisms of deposition and release. *J. Membr. Sci.* 2004, 244, 151−165.

(29) Busnaina, A.; Taylor, J.; Kashkoush, I. Measurement of the adhesion and removal forces of submicrometer particles on silicon substrates. *J. Adhes. Sci. Technol.* 1993, 7, 441−455.

(30) Burdick, G. M.; Berman, N. S.; Beaudoin, S. P. Describing hydrodynamic particle removal from surfaces using the particle Reynolds number. *J. Nanopart. Res.* 2001, 3, 453−465.

(31) Saffman, P. G. The lift on a small sphere in a slow shear flow. *J. Fluid Mech.* 1965, 22, 385−400.

(32) Saffman, P. G. Correction to "The lift on a small sphere in a slow shear flow. *J. Fluid Mech.* 1968, 31, 624.

(33) Akhatov, I. S.; Hoey, J. M.; Swenson, O. F.; Schulz, D. L. Aerosol focusing in micro-capillaries: Theory and experiment. *J. Aerosol Sci.* 2008, 39, 691−709.

(34) Derjagin, B. V.; Landau, L. D. Theory of the stability of strongly charged lyophobic sols and of the adhesion of strongly charged particles in solutions of electrolytes. *J. Acta Physicochim. URSS* 1941, 14, 633−662.

(35) Gregory, J. Approximate expressions for retarded Van der Waals interaction. *J. Colloid Interface Sci.* 1981, 83, 138−145.

(36) Elimelech, M.; Gregory, J.; Jia, X.; Williams, R. A. *Particle Deposition and Aggregation*; Butterworth-Heinemann: Boston, 1995.

(37) Israelachvili, J. *Intermolecular and Surface Forces*; Academic Press: London, 2006.

(38) Landau, L. D.; Lifshitz, E. M. *Statistical Physics, Part 1*; Pergamon Press: Oxford, 1980; Course in Theoretical Physics, Vol. 5.

(39) Schramm, L. L.; Mannhardt, K.; Novosad, J. J. Electrokinetic properties of reservoir rock particles. *J. Colloids Surf.* 1991, 55, 309−331.

(40) Elzo, D.; Huisman, I.; Middelink, E.; Gekas, V. Charge effects on inorganic membrane performance in a cross-flow microfiltration process. *Colloids Surf., A* 1998, 138, 145−159.

(41) Faibish, R. S.; Elimelech, M.; Cohen, Y. Effect of interparticle electrostatic double layer interactions on permeate flux decline in crossflow membrane filtration of colloidal suspensions: An experimental investigation. *J. Colloid Interface Sci.* **1998**, *204*, 77−86.

(42) Hong, S.; Faibish, R. S.; Elimelech, M. Kinetics of Permeate Flux Decline in Crossflow Membrane Filtration of Colloidal Suspensions. *J. Colloid Interface Sci.* **1997**, *196*, 267−277.

(43) Song, L.; Singh, G. Influence of various monovalent cations and calcium ion on the colloidal fouling potential. *J. Colloid Interface Sci.* **2005**, *289*, 479−487.

(44) Tarabara, V. V.; Koyuncu, I.; Wiesner, M. R. Effect of hydrodynamics and solution ionic strength on permeate flux in cross-flow filtration: direct experimental observation of filter cake cross-sections. *J. Membr. Sci.* **2004**, *241*, 65−78.

(45) Derjaguin, B. V.; Muller, V. M.; Toporov, Y. P. Effect of contact deformations on the adhesion of particles. *J. Colloid Interface Sci.* **1975**, *53*, 314−326.

(46) Zhang, P.; Fan, C.; Lu, H.; Kan, A. T.; Tomson, M. B. Synthesis of Crystalline-Phase Silica-Based Calcium Phosphonate Nanomaterials and Their Transport in Carbonate and Sandstone Porous Media. *Ind. Eng. Chem. Res.* **2011**, *50*, 1819−1830.

(47) Ramarao, B. V.; Tien, C. Approximate Analysis of Fine-Particle Retention in the Cake Filtration of Suspensions. *Ind. Eng. Chem. Res.* **2005**, *44*, 1424−1432.

(48) Tien, C. *Introduction to Cake Filtration: Analyses, Experiments and Applications*; Elsevier: Amsterdam, 2006.

(49) Yuan, H.; Nielsen, S.; Shapiro, A.; Bedrikovetsky, P. A New Comprehensive Approach for Predicting Injectivity Decline during Waterflooding. SPE 154509, Presented at SPE Europec/EAGE Annual Conference, Copenhagen, Denmark, June 4−7, 2012.

(50) Zhang, W.; Tang, X.; Weisbrod, N.; Guan, Z. A review of colloid transport in fractured rocks. *J. Mt. Sci.* **2012**, *9*, 770−787.

(51) Kahrobaei, S.; Farajzadeh, R.; Suicmez, V. S.; Bruining, J. Gravity-Enhanced Transfer between Fracture and Matrix in Solvent-Based Enhanced Oil Recovery. *Ind. Eng. Chem. Res.* **2012**, *51*, 14555−14565.

(52) Farajzadeh, R.; Andrianov, A.; Zitha, P. L. J. Investigation of immiscible and miscible foam for enhancing oil recovery. *Ind. Eng. Chem. Res.* **2009**, *49*, 1910−1919.

(53) Andrianov, A.; Farajzadeh, R.; Mahmoodi Nick, M.; Talanana, M.; Zitha, P. L. J. Immiscible foam for enhancing oil recovery: bulk and porous media experiments. *Ind. Eng. Chem. Res.* **2012**, *51*, 2214−2226.

(54) Ishigami, T.; Fuse, H.; Asao, S.; Saeki, D.; Ohmukai, Y.; Kamio, E.; Matsuyama, H. Permeation of Dispersed Particles through a Pore and Transmembrane Pressure Behavior in Dead-End Constant-Flux Microfiltration by Two-Dimensional Direct Numerical Simulation. *Ind. Eng. Chem. Res.* **2013**, *52*, 4650−4659.

(55) Kim, A. S.; Liu, Y. Irreversible chemical potential and shear-induced diffusion in cross-flow filtration. *Ind. Eng. Chem. Res.* **2008**, *47*, 5611−5614.